

This work was written as part of one of the author's official duties as an Employee of the United States Government and is therefore a work of the United States Government. In accordance with 17 U.S.C. 105, no copyright protection is available for such works under U.S. Law.

Public Domain Mark 1.0

<https://creativecommons.org/publicdomain/mark/1.0/>

Access to this work was provided by the University of Maryland, Baltimore County (UMBC) ScholarWorks@UMBC digital repository on the Maryland Shared Open Access (MD-SOAR) platform.

Please provide feedback

Please support the ScholarWorks@UMBC repository by emailing scholarworks-group@umbc.edu and telling us what having access to this work means to you and why it's important to you. Thank you.

Quasi-Periodic Transverse Plasma Flow Associated With an Evolving MHD Vortex Street in the Outer Heliosphere

EDOUARD SIREGAR, D. AARON ROBERTS, AND MELVYN L. GOLDSTEIN

Laboratory for Extraterrestrial Physics, NASA Goddard Space Flight Center, Greenbelt, Maryland

We study a transverse ("meridional" in heliocentric coordinates) plasma flow induced by the evolution of a Karman vortex street using a Chebyshev-Fourier spectral algorithm to solve both the compressible Navier-Stokes and magnetohydrodynamic (MHD) equations. The evolving vortex street is formed by the nonlinear interaction of two vortex sheets initially in equilibrium, such as are naturally found either side of the heliospheric current sheet at solar minimum. We study spatial profiles of the total plasma velocity, the density, the meridional flow angle and the location of sector boundaries and find generally good agreement with Voyager 2 measurements of quasi-periodic transverse flow in the outer heliosphere. The pressure pulses associated with the meridional flows in the simulation are too small, although they are correctly located, and this may be due to the lack of any "warp" in the current sheet in this model. A strong, flow-aligned magnetic field, such as would occur in the inner heliosphere, is shown to lead to weak effects that would be masked by the background interplanetary turbulence. We also study the plasma and magnetic transport resulting from the meridional flow, and find that deficits of magnetic quantities do occur near the ecliptic and that while the effect is relatively small, it is in general agreement with the most recent analysis of 'flux deficit' in the outer heliosphere.

1. INTRODUCTION

The Plasma Science experiment on board Voyager 2 revealed a surprising quasi-periodic meridional solar wind plasma flow in the outer heliosphere [Lazarus *et al.*, 1988; McNutt, 1988] during a long interval near solar minimum. From 1986 to early 1988, Voyager 2 was in the ecliptic and near the heliospheric equatorial plane (within 2°) and located between 20 AND 25 AU. The period of flow variations was close to 25.5 days or about one solar rotation period, and the deflection angle of the flow was as much as 5°. Over such large distances, the observation of this regularity in the turbulent solar wind is remarkable.

The high-speed streams flowing either side of the heliospheric current sheet provide a natural source for the periodicity of the N-S variations in the flow. However, as with the problem of interplanetary turbulence [Roberts and Goldstein, 1991] a significant question is the degree to which the streams lead to compressive effects as compared to shear effects. While high-speed wind will compress slower flow in front of it, it is not clear that this should lead to meridional excursions of the flow. The detailed model of Pizzo and Goldstein [1987] that uses the pressure built up by the streams to drive meridional flow predicts that there will be two N-S excursions of the flow vector each solar rotation, and these will both be accompanied by latitude variations. Although two maxima are observed in the solar wind speed for each period of the pattern, only one cycle of transverse flow is seen and it is nearly always perpendicular to the ecliptic; this implies that although the Pizzo and Goldstein model undoubtedly captures some of the features of stream evolution, it is missing an important ingredient. McNutt [1988] proposed another approach to the pressure-driven scenario; he achieves rough qualitative, but not detailed, agreement with observations.

It is possible that the problems with the pressure-driven models can be solved—for example, the two deflections per solar rotation may become one as the streams form merged interaction regions—but these models could fail in detail due to their neglect of the shear flow dynamics. Simple models that incorporate this aspect of the flow and which are consistent with the speed and flow direction periodicities have been presented by Burlaga [1990] and Veselovsky (preprint 1989) who suggested that the formation of a heliospheric vortex street leads to the unusual meridional solar wind flows. The Burlaga model is based on two-dimensional infinite line vortices that alternate in sign and lie on alternate sides of the heliographic equator (a "Karman vortex street" as observed in flows behind a cylinders for a wide variety of parameters). This static model suffers from the existence of singularities in the flow and from the lack of a demonstration that the flow will actually break up into the required vortices. The vortex street model best fitting the observations has vortices separated by about 6 AU along the mean stream direction. Veselovsky also suggests the existence of vortices in the outer heliosphere, and derives his conclusion using a first order solution to the polytropic gas dynamic equations. Combined observations from Pioneer 11 and Voyager 2 show that a velocity shear of 200 km/s/15° exists when one moves from the heliospheric equator to higher latitudes [Gazis *et al.*, 1989]. The shear should be approximately symmetric about the equator. As we shall show below, perturbations such as those likely to be provided by the high-speed streams on either side of the warped current sheet region applied to this type of flow configuration can create Karman vortex streets.

In addition to its consistency with the observations, the vortex street model is also attractive in terms of fluid dynamical considerations. Shear flows (such as jets, free convection shear, boundary layers) at high Reynolds numbers become fully turbulent not too far downstream. The only exception is the Karman vortex street that shows a strong stability. Experiments done at various Reynolds numbers (based on the diameter of a cylinder) show that periodic vortex

Copyright 1993 by the American Geophysical Union.

Paper number 93JA01032.
0148-0227/93/93JA-01032\$05.00

shedding occurs at all Reynolds numbers tried experimentally (up to 10^7 [e.g., Tritton, 1977]). As the Reynolds number becomes very large, the regularity of the staggered array of vortices can be somewhat lost, but quasi-periodic features still remain making the vortex street description more relevant than a fully turbulent flow.

In this paper, we study local flow profiles given by a compressible magnetohydrodynamic (MHD) computational model of an evolving two-dimensional compressible Karman street. The lack of third dimensions precludes possibly important effects such as vortex stretching and the interaction with magnetic tearing modes. We are currently working on such aspects of the problem. We analyze spatial variations of plasma parameters that can be related to Voyager 2 observations. This model (presented in section 2) allows us to address questions such as the correlation between density/pressure fluctuations and other parameters, and the effect of compressibility on the growth of the relevant instabilities. In section 3 we address the question of plasma and magnetic transport from the heliospheric equator associated with this meridional flow. We explore in section 4 the origin and maintenance of such Kármán vortex systems and the influence of a magnetic field pressure on them. In section 5 compressibility effects and the transport of magnetic quantities by the dynamics of vortices are studied using simple transport equations for magnetic quantities. Finally, we briefly discuss in section 6 processes which could become significant on scales longer than the inertial nonlinear time scales.

In our computations the vortex street is formed out of the interactions of two perturbed equilibrium vortex sheets. We primarily study the compressible Navier-Stokes fluid case with an infinitesimal passive magnetic field used as a tracer. This case provides a reasonable approximation to the flow in the outer heliosphere because the mean magnetic field is transverse to the flow and thus will not inhibit the growth of perturbations with radially aligned wave vectors. As mentioned by Burlaga, a conclusive test for the vortex street hypothesis would be provided by simultaneous observations from several spacecraft at different latitudes (corresponding to about a vortex size) about the heliospheric current sheet.

2 THE MODEL HELIOSPHERIC SOLAR WIND PLASMA FLOW

In the current picture of the outer heliospheric equatorial solar wind, the velocity of the supersonic, super-Alfvénic plasma increases away from the heliospheric current sheet (which is a skewed surface near the heliospheric equator). In periods of low solar activity, the velocity increases from 400 to 700 km/s as one moves north or south of the current sheet. It is known from theory and computations that certain growing modes can induce two neighboring vortex layers to strongly interact and eventually form a Karman street of vortices. The rotating, time varying “boundary condition” (presumed to lie at some point near a solar coronal hole) can give rise to a broad spectrum of perturbations that can include the growing modes of the interacting vortex sheets. In this manner, coherent modes could tap the free energy available within the shear layers to form regular patterns of vortices above and below the heliospheric current sheet. In particular, Lazarus *et al.* [1988] find that the plasma flow near 1 AU contains high-speed streams above and below the equatorial plane that are about 180° out of phase, and these will lead to flows that alternately

are faster above and below the plane when observed along a radial line. This is the type of perturbation with which we initialize our computations.

We study the interaction of a coupled pair of vortex sheets using a Chebyshev-Fourier algorithm to solve the two dimensional compressible Navier-Stokes equations and the corresponding MHD equations. We focus our attention on processes related to local plasma shear that exist in the comoving solar wind frame. The physical processes related to the spherical symmetry of the solar wind flow are small if we consider time intervals during which the plasma travels a short distance compared to the distance to the Sun. Azimuthal effects cannot be addressed here, but the Voyager 2 observations do not indicate a periodic azimuthal flow with the magnitude of the meridional flow. We study large enough time and space scales for MHD theory to be applicable and use a scalar pressure and a constant, isotropic kinematic viscosity. There is no numerical modeling of dissipation other than the normal Navier-Stokes terms. The four Eulerian variables used are the density ρ , the two velocity components (u_x, u_y) and the magnetic vector potential a . A polytropic transformation equation is used. Such polytropic model is used as a first approximation to concentrate on dynamical effects and leave energy and transport effects as corrections. Large scales (inertial zone wave numbers) are well described by this model, and energy considerations become imperative near the dissipation regions.

The dimensional density, length, and velocity variables are respectively $\rho = \rho_0 \rho^+$, $x = L_0 x^+$, $y = L_0 y^+$, $u = u_0 u^+$. The quantities with subscripts zero are characteristic dimensional scales of the problem, and the + superscripted variables are dimensionless. The dimensional time is $t = (L_0/u_0)t^+$. The Mach number is $M_a = u_0/c_0$, with the characteristic polytropic sound speed $c_0 = c(\rho=\rho_0) = \rho_0^{(\gamma-1)/2}$. The Alfvén Mach number is $M_m = u_0/c_a$, with the characteristic Alfvén speed c_a . The fluid and magnetic Reynolds numbers are $R_e = u_0 L_0 \rho_0 / \mu$ and $R_m = u_0 L_0 \rho_0 / \eta$, respectively. The range of the dimensionless spatial variables is $[0, 2\pi]$ for x^+ and $[-1, 1]$ for y^+ . By dropping the plus for nondimensional scaled variables, the dimensionless MHD equations for two-dimensional flows become

$$\partial_t \rho = -\bar{\nabla} \cdot (\rho \bar{\mathbf{u}}) \quad (1)$$

$$\begin{aligned} \partial_t \bar{\mathbf{u}} = & -\bar{\mathbf{u}} \cdot \bar{\nabla} \bar{\mathbf{u}} - \frac{1}{\gamma \rho M_a^2} \bar{\nabla} \rho^\gamma \\ & + \frac{R_e}{\rho} [\nabla^2 \bar{\mathbf{u}} + \frac{1}{3} \bar{\nabla} (\bar{\nabla} \cdot \bar{\mathbf{u}})] - \frac{1}{\gamma \rho M_m^2} \bar{\nabla} a (\nabla^2 a) \end{aligned} \quad (2)$$

$$\partial_t a = \bar{\mathbf{u}} \cdot \bar{\nabla} a + \frac{1}{R_m} \nabla^2 a \quad (3)$$

For convenience, we use inflexional hyperbolic tangent velocity profiles described by the equations below for our equilibrium model vortex layers. Details of the velocity profile are of little importance for stability considerations when the perturbation wavelengths used are much larger than the characteristic width of the vortex layers. We use very thin vortex layers and refer to them as “sheets” and perturb them with the fastest growing modes that can exist within the computation domain. Tests done with pure noise and no other perturbation lead to a similar vortex street. The centers of our initial equilibrium vortex sheets are located at x_{01} and x_{02}

along the cross-stream x direction. The mean velocity \bar{u}_0 has components $u_{0x} = 0$ and u_{0y} has components

$$\begin{aligned} u_{0y}(x) &= u_0 + u_{01} \tanh[2\pi(x-x_{01})/\delta_0], & x < \pi, \\ u_{0y}(x) &= u_0 + u_{02} \tanh[2\pi(x-x_{02})/\delta_0], & x > \pi \end{aligned}$$

where the velocity normalization coefficients are $u_{01} = u \tanh[2(2\pi - x_{01})/\delta_0]$ and $u_{02} = u \tanh[2(2\pi - x_{02})/\delta_0]$. The Mach number is defined by the velocity difference across the sheets; i.e., $Ma = 2u_0/c_0$. In the pure Navier-Stokes fluid and the case with an infinitesimal magnetic field, the initial density is taken to be uniform, normalized to unity throughout the flow, which makes the initial sound velocity also equal to unity. In relation to the solar wind analysis, the x direction is the north-south (N-S) or meridional direction, while y is the direction comoving with the solar wind plasma.

The mean velocity profile $u_{0y}(x)$ is an exact solution of the Navier-Stokes and it is also taken as an initial condition. In the absence of noise or superimposed perturbation, this profile is stationary, apart from the slow diffusive broadening of the sheets on a dissipative time scale.

We use a tiny passive magnetic field to locate the heliospheric current sheet and evaluate the transport of magnetic quantities under a fluid dominated dynamics. In order to preserve the x periodicity of the flow, the initial magnetic field is chosen to be a Fourier expansion approximation to a field that has values zero, $+b_y$, $-b_y$, zero as one proceeds along the cross-stream x direction from 0 to 2π . This gives rise to two small outer current sheets and a larger central current sheet.

We use four (most unstable) modes to study the effects of the large and medium scales in the Karman street on the meridional transport of plasma quantities. Low resolution numerical experiments done with white noise (and no wavy perturbations) lead to a very similar vortex street configuration, but in a much longer time. Earlier studies done with discrete point vortices [Siregar et al., 1992] lead to this result. An antisymmetric perturbation is used to initiate a cross-stream displacement of the two sheets as well as an inhomogeneity in the strength of vorticity along the vortex sheets. The initial characteristic lengths in the flow are the distance $d = x_{02} - x_{01}$ between the two sheets, the perturbation wavelength $\lambda = 2\pi/m$ and the shear layer width δ_0 . For given width δ_0 the dimensionless ratio $S = d/\lambda$ will control the interaction strength between the sheets. The parameter S and the phase difference between the two perturbations along each sheet are two important bifurcation parameters for the time asymptotic solution of the flow, but this aspect is not discussed in this paper.

The computational algorithm used is a spectral collocation method [Gottlieb and Orszag, 1977]. Spectral methods can be understood as a generalization of the separation of variables method and can be applied to complex nonlinear problems. Dependent variables are represented in each spatial direction x and y by a global expansion in terms of orthogonal Chebyshev $T_n(y)$ and Fourier $\exp[-ikmx]$ functions. The dependent variables q are represented as $q(x, y, t) = \sum \sum a_{mn}(t) \exp[-ikmx] T_n(y)$ and we use a second order Adams Bashforth-Crank Nicholson (ABCN) semi-implicit time scheme. Time marching is done in the spectral Fourier-Chebyshev space.

Verifications of the computational algorithm's performance during the evolution of the vortex street are made by examining the behavior of some of the ideal global invariants of the fluid (total mass, momentum, and energy), as well as the dissipative evolution of the enstrophy Z (defined below) and energy

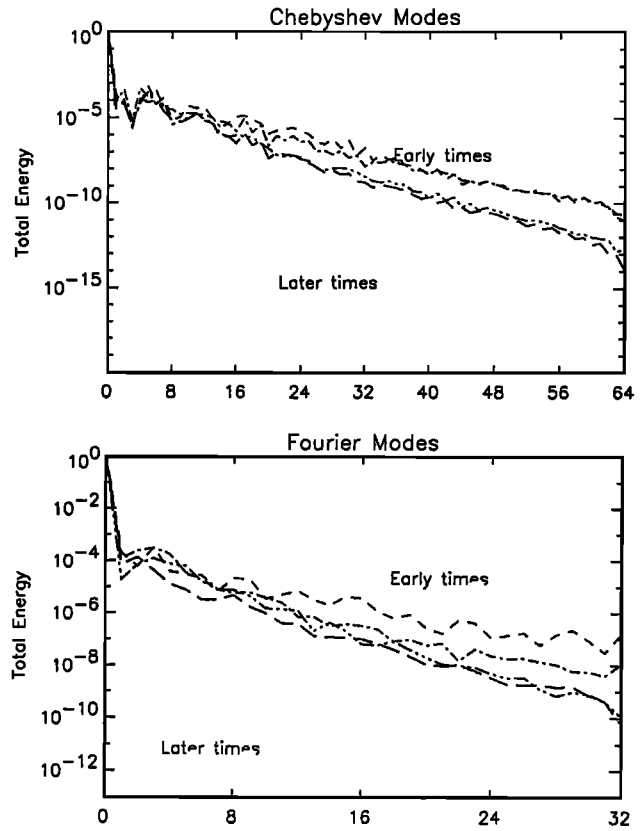


Fig. 1. Time evolution total energy spectra in the streamwise y direction (above) and in the cross-stream x direction (below). The higher modes are damped by more than 5 orders of magnitude. A quasi-steady spectrum is observed at the low Chebyshev wave numbers, corresponding to the slowly evolving street of vortices. The spectra are renormalized to the mean plasma flow energy.

spectra. With zero dissipation, a test run using 10,000 steps conserves total energy ($\Delta E/E = 3 \times 10^{-4}\%$), mass and momentum (better than one part in 10^6). The typical time evolution energy spectra are shown in Figures 1a and 1b for computations with a small dissipation. Each spectrum is averaged over the other direction (cross-stream N-S Fourier- x and streamwise Chebyshev- y directions respectively). The highest wavenumbers are damped by more than six orders of magnitude during the total computation time that spans from 0 to 30. There is a quasi-steady evolution at lower Chebyshev modes as most of the energy goes to the large scales in the coherent eddies. The cascade processes of energy and vorticity can also be inferred by examining the effects of dissipation on these respective quantities. Figures 2a and 2b show the time evolution of mean total energy in the flow and the total enstrophy Z defined as $(1/2)\langle \omega^2 \rangle$ (where $\langle \rangle$ is an ensemble average calculated here as a spatial average). In a manner similar to that seen in turbulent two-dimensional incompressible flows, the direct enstrophy cascade towards smaller scales is faster than the energy cascade. This is reflected in the fact that the mean total energy decreases by a small amount ($\Delta E/E = 0.87\%$) at this Reynolds number (10^3), while enstrophy which cascades to small scales is strongly damped ($\Delta Z/Z = 92\%$). Thus energy resides mostly in the large scales and remains almost constant, while enstrophy flows through the dissipation scales and is strongly damped. In this study, the boundary handling capabilities of the Chebyshev

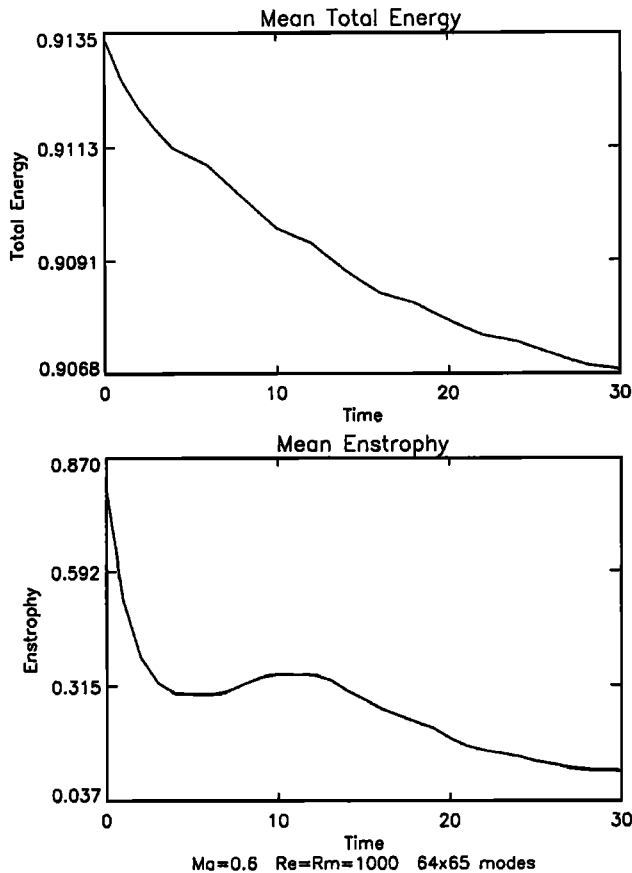


Fig. 2. (a) Total plasma energy (note $\Delta E/E = 0.88\%$). Most of the energy cascades towards the large scales of the main vortices so that the damping of energy due to viscous stresses remains small at this Reynolds number (10^3). (b) Total enstrophy Z showing a large relative decrease ($\Delta Z/Z = 92\%$). This follows from the direct enstrophy cascade to small dissipation scales.

expansions are not used for reasons described below and the flow is periodic in both directions. Time marching is done in Fourier-Chebyshev spectral space and nonlinear terms are calculated in configuration space by using fast Fourier and cosine ("Chebyshev") transforms, making this a pseudospectral algorithm.

We now discuss the choice of flow geometry and the influence of boundary conditions. We tested an identical plasma flow using the Chebyshev polynomials and an algebraic map in the direction transverse to the flow. The coordinate map transforms the $[-1, +1]$ computational domain into an infinite physical domain in both directions. The results are almost identical to the present calculation in periodic geometry. The infinite-domain flow contains, however, an arbitrary scale parameter. The effects of such map on the physics and numerics is not clear to us at this point (although it does not seem to introduce particular problems). Therefore a flow in purely periodic geometry is used for this paper.

To further assess the importance of boundary conditions in the cross-stream direction, we have tested "channel" type flow configurations with no-slip boundary conditions at the channel wall. After the linear growth phase, the vortex flow becomes significantly different from the one presented here. Vorticity generated at the two boundary layers near the walls begins to interact with the vortex street, forming connecting filaments

between coherent vortices in the street and vorticity in the boundary layers. These boundary conditions, however, are not relevant to the solar wind plasma flow. Stress-free channel boundary conditions will be tested in future studies involving warped current sheets. Note also that in the model presented here, the perturbation wavelength along the flow direction is completely determined by the solar rotation period and the solar wind speed. Such "initial" flow configuration then moves outward [Siregar *et al.*, 1992] and a periodic geometry is a good representation of the situation along the flow direction.

3. PARAMETER PROFILES THROUGH A QUASI-STEADY MHD KARMAN VORTEX STREET

To get a clearer picture of the solar wind dynamics near the heliospheric current sheet, we study a number of plasma variables along radial trajectories in the neighborhood of the current sheet. The model contains the parameters S , Ma and Re defined above. The sensitivity of the flow to these parameters will be considered further elsewhere, but here, we give a brief account. The ratio S determines the interaction strength between the two sheets and the detailed nature of the sheet interaction. The time required to reach the final stages of evolution is longer for larger values of S . Here we present results with $S = 0.075$. The results are qualitatively unchanged on these time scales, while S remains below about 0.3. Above that critical value and on these time scales, the two vortex sheets are far apart and evolve almost independently. In this case, the merging of the vortices along each shear layer is the dominant process. The Mach number Ma influences the axisymmetry of the vortices formed and the degree of filamentation of vorticity. The Reynolds number Re is chosen as high as possible (10^3) for a stable code run given the intensity of the turbulence in the flow and the number of modes in the computations. We now present the spatial profiles of plasma parameters, chosen for comparison with previous models and the Voyager 2 observations.

Before examining any further the time evolution aspect we present the scaling of the parameters T , U and S , so that a connection can be made with other models and the solar wind. The time scale unit T_0 is based on the vortex spacing λ (i.e., the initial perturbation wavelength) and the velocity difference $2u$ across the initial equilibrium vortex sheets. Hence, we take $T = t/T_0 = 2ut/\lambda$, where t is the nondimensional computation time used in the equations. The total velocity $U(y) = (u_x^2 + u_y^2)^{1/2}$ is given in units of the mean sound speed $c = 1$ in the computation domain (i.e., it is a Mach number). The space scale ratio $S = d/\lambda$ defined in section 2, controls the interaction strength between the vortex sheets.

We now use the above to scale the velocity and distance. The vortex street model has a spacing λ related to the period of the meridional x-directed flow of about 25.5 days, giving λ a value near 6 AU [see Burlaga, 1990]. In the Chebyshev-y direction, this computational length is 2, so that one unit of nondimensional length corresponds to 3 AU. Since we have $S = 0.075$, that makes the initial distance d between the vortex sheets equal to 0.45 AU. The white vorticity contour plots superimposed on the gray density background in Figure 3 illustrate a typical evolution of the vortex street between $T = 0$ and $T = 24$. For later times, when the Karman street has evolved into a quasi-steady state (e.g., last frame in Figure 3) the spacing length d , perpendicular to the flow, between the centers of opposite vortex rows is about 2.5 AU.

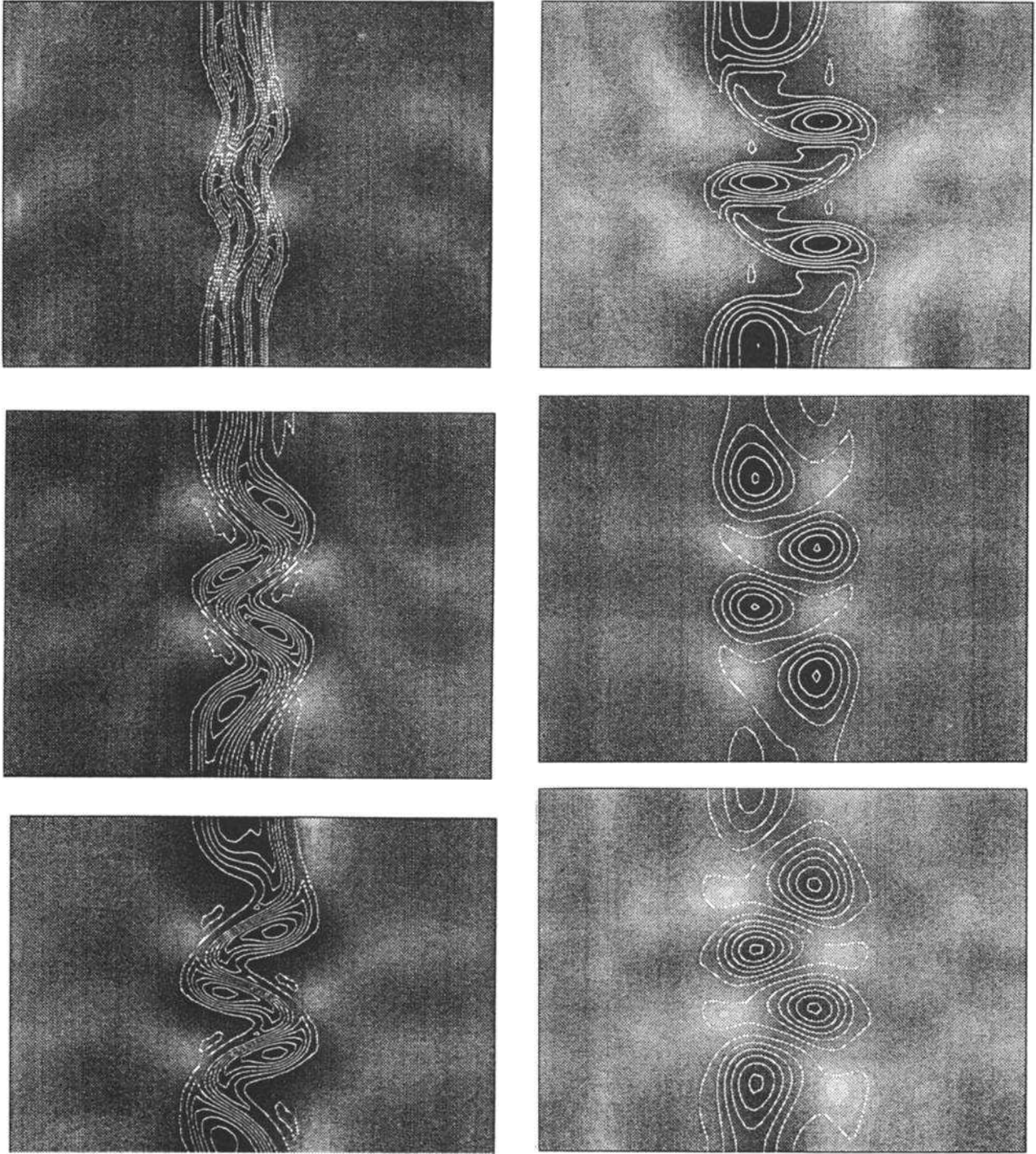


Fig. 3. Typical evolution of the street. White vorticity contours are overlaid on the grey density background, and T varies from 1.08 to 24.

If one nondimensional unit of velocity is taken to be equal to 250 km/s, then the initial central plasma around the current sheet region has a speed of 425 km/s and the regions outside have a speed of 575 km/s in these computations. Since $T = t/T_0 = 2ut/\lambda$, we can translate the nondimensional time t into days by taking the dimensional unit T_0 in days, by using $2u = 575 - 425 = 150$ km/s and $\lambda = 6$ AU $= 9 \times 10^8$ km. The first signs of double maxima profiles for U occur around $T = 1.08$. In the above units, this corresponds to 76 days, which at 425 km/s corresponds to about 18.5 AU. At that stage ($T=1.08$),

however, the vortex street is still early in its evolution toward a quasi-steady state (see Figure 4).

We plot profiles of the density, the total velocity $U(y) = [u_x^2 + u_y^2]^{1/2}$ and the meridional angle $\vartheta(y) = \arctan[u_x/U]$ along lines in the streamwise (y) direction. The profiles given in this section are at a given time when the vortex street is in a slowly evolving state ($T = 2.16$ in Figure 5). The cut is done along the symmetry axis between the vortex streets (solid lines in Figure 6), or in a position offset ("north") from that axis by about 0.3 AU (dashed lines). (See section 4 for the scaling of

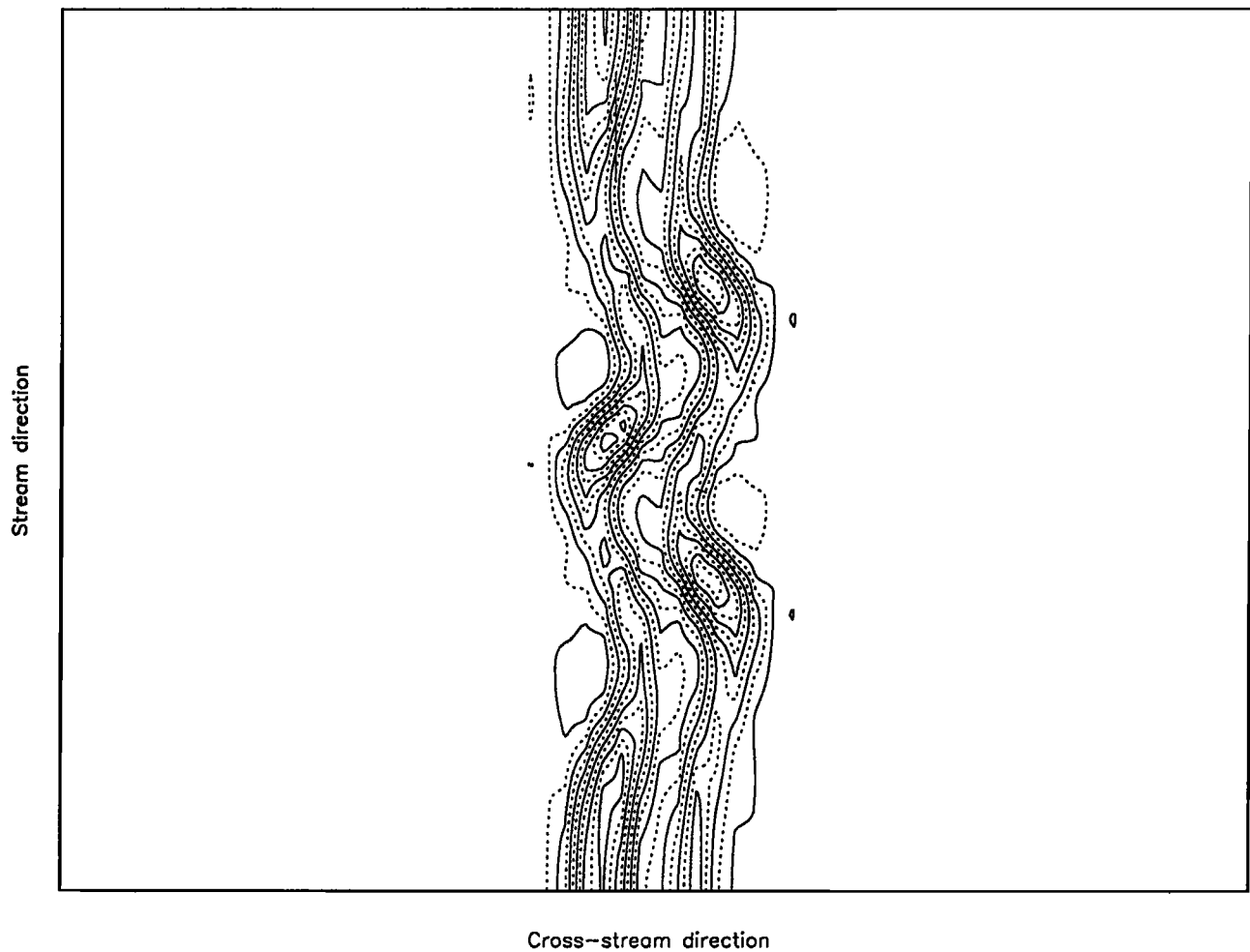


Fig. 4. Vorticity contours at $T=1.08$ when the characteristic plasma profiles first appear.

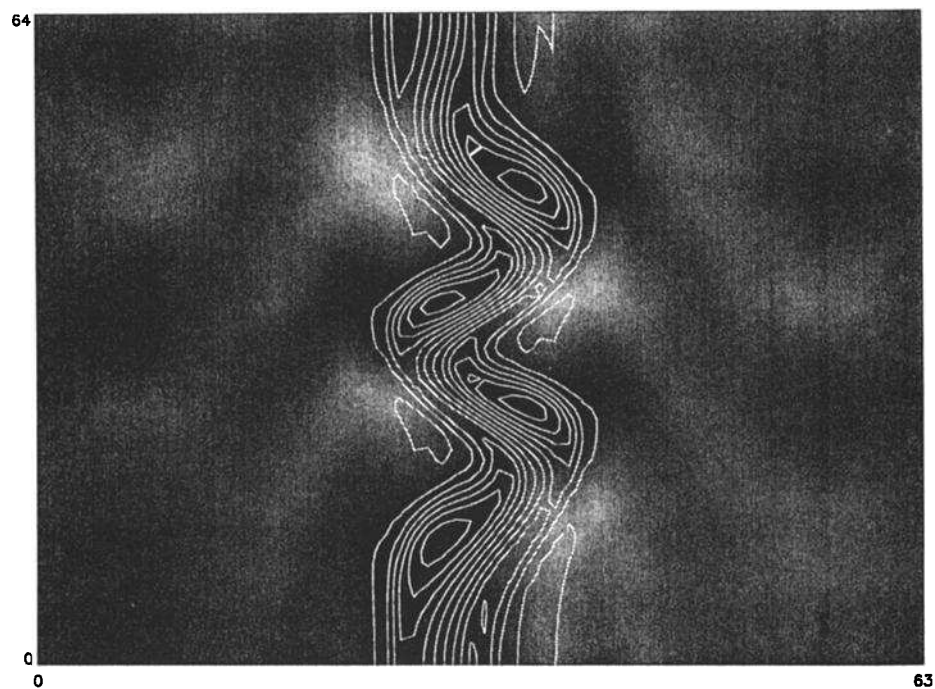


Fig. 5. White contours of vorticity over a grey density background at $T=2.16$. The low pressure/density plasma cavities (in black) are embedded in the low pressure/density expanding central region.

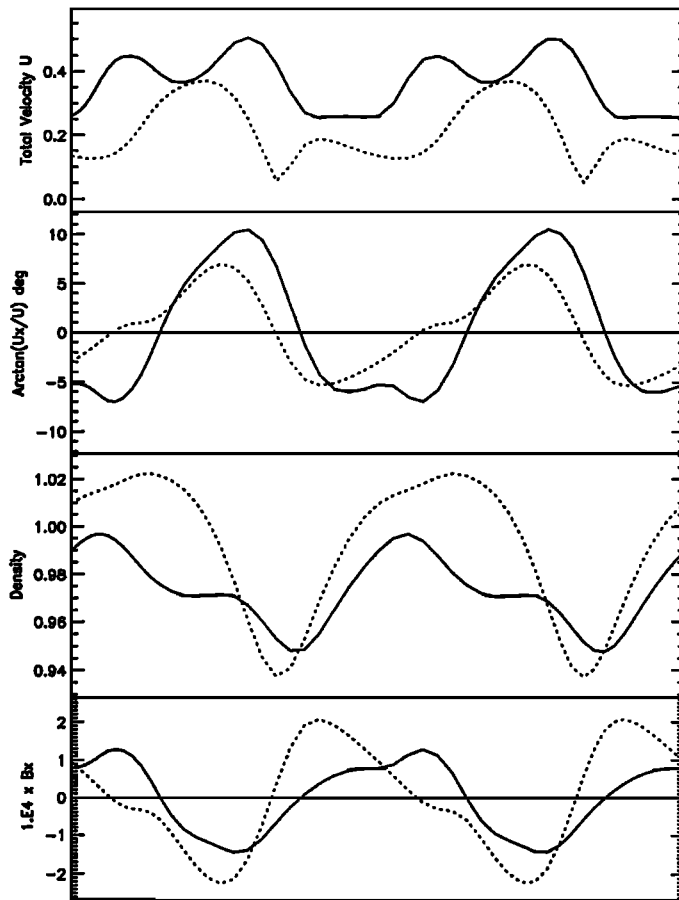


Fig. 6. Plasma parameter profiles at $T=2.16$ are taken along the y axis, at the center of the cross-stream x direction (solid) and through the center of vortices (dashed). From top to bottom the profiles show the total plasma velocity in Mach units, the meridional angle $\text{Arctan}(u_x/U)$ in degrees, the density (and pressure) variations, and the transverse component of the magnetic field. The structure of maxima and correlations are not very sensitive to the exact heliocentric latitude of the trajectory through the street.

variables.) The plotted values of U are given in terms of fractions of mean sound speed units, that is, by a Mach number. The periodic variations of the total velocity U and the meridional flow angle are clear. The amplitude of the transverse velocity is in accord with observations, as is the occurrence of only one cycle per cycle of the perturbation. As in Burlaga's simple line vortex model, the total velocity exhibits two maxima per period. The difference is that here the maxima are not of equal intensity, consistent with the Voyager 2 observations.

Our compressible MHD model provides information on density/pressure profiles. This allows a test of the consistency of the vortex street model with the observed correlations between variables related to the vortex patterns and pressure gradients. In this polytropic model, variations of pressure are strictly correlated to density variations. Along the symmetry axis of the vortex street, or close to it, the pressure/density maxima are well correlated to the increase in total velocity U (see Figure 6). The density (pressure) has one maximum for each period of the total velocity (which has a "two maxima" structure during that time). This is consistent with suggestions that pressure can contribute to the driving of the meridional flow, or is at least intimately related to it, and agrees with the

observations presented by Lazarus *et al.* [1988]. The magnitude of the pressure variations is too small, but increased pressure pulses would be expected if the geometry included a "warp" of the heliospheric current sheet; in the present model, the high-speed flows never directly encounter the slower flow between them, and thus compression is suppressed.

Pressure/density cavities are strongly correlated with the vortex structures along the Karman street. This is mainly due to the inertial ejection of plasma from the spinning vortices, a process that continues until a pressure-centrifugal quasi-equilibrium is reached. The vortices by themselves do not globally transport mass and magnetic field, but the combined effects of vortex/antivortex repulsion and inertial plasma ejection from vortices create a central region of expansion, transporting plasma and magnetic energy (see below) away from that region. Figure 5 shows that the density is lower than the mean value 1 near the central current sheet region.

Figure 6 shows that for each period in the flow the cross-stream (x) component of the magnetic field undergoes two sign reversals, as observed by Lazarus *et al.* [1988]. The reversals tend to be near the points of zero transverse velocities while the data show a displacement between these points; whether or not this could also be a consequence of a warp in the current sheet is unknown.

To test whether a vortex street would tend to develop in the inner regions of the heliosphere, we increased the magnetic field by along the stream y direction. Farther out from the Sun, this b_y component tends to zero as the interplanetary magnetic field turns perpendicular to the stream direction. The IMF then has little influence on the stability of the shear flow and the above fluid description is valid. When the initial ratio of magnetic E_m to fluid E_f (internal + kinetic) energies is up to about 10^{-3} , the vortex structures along the street are virtually unchanged and the profiles are very similar to those of the near zero magnetic field limit. When the initial ratio E_m/E_f is increased to about 10^{-2} the vortices that are formed appear to be squeezed through their center (Figure 7) and there is a quasi-periodic exchange of energy between the fluid and the magnetic field energies. As expected, when the initial ratio E_m/E_f becomes large enough (though still small compared to 1), and with the magnetic field oriented parallel to the flow, it becomes stabilizing and inhibits the development of the vortex street. It would not be observable in the inner heliosphere where the energy of the flow-aligned field is comparable to the free shear energy in the solar wind.

4. DYNAMICS OF VORTICITY

To understand the complex interplay between the vorticity, the density/pressure and magnetic quantities in the street we have to undertake a detailed analysis of the equations governing the flow. Because the magnetic field is being used as a tracer, we can start by investigating fluid quantities. The first issue we address is what creates the pressure/density cavities in the vortices? In fact, there are well known free vortex solutions to the Navier-Stokes compressible flow. Axisymmetric, or nonelliptical free vortex solutions satisfy a pressure centrifugal equilibrium given by $\partial p / \partial r = \rho u^2 / r$, where r is the radial distance to the center of the vortex. Steady elliptical free vortex solutions also exist. To completely specify a compressible vortex solution additional information is needed. For example, a line vortex in a polytropic flow with a velocity profile $u(r) = a/r$ has a density profile

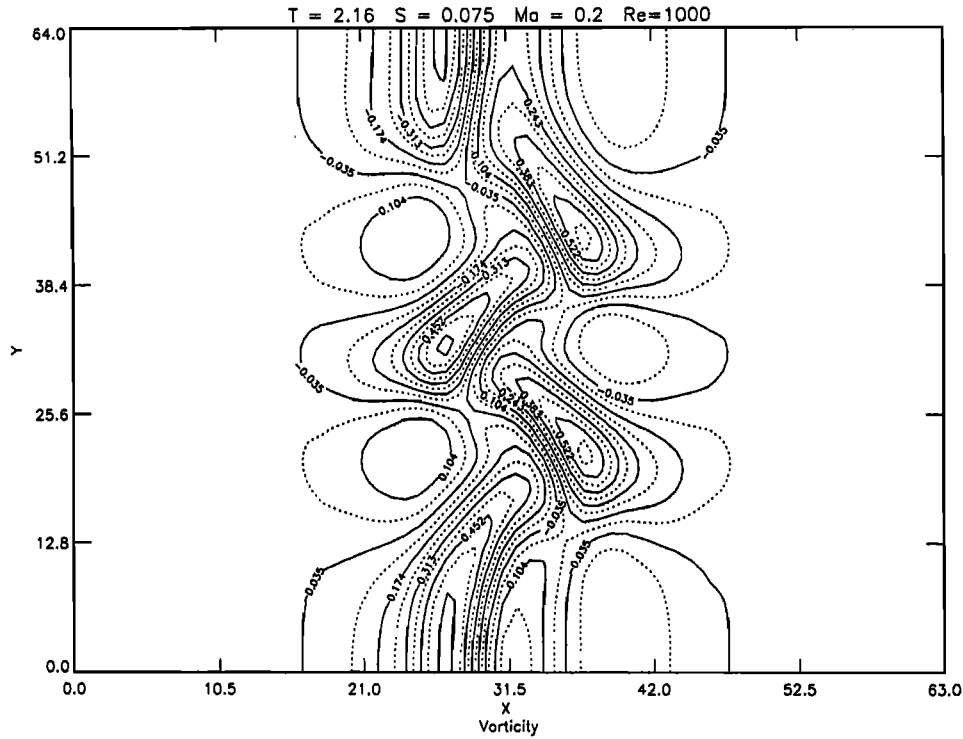


Fig. 7. Effect of a small magnetic field energy with a flow aligned field. The initial ratio E_m/E_f of total magnetic to total fluid (internal+kinetic) energies is about 10^{-2} .

$$\rho(r) = [(\gamma(\gamma-1))[-a^2/2r^2 + C]^{1/\gamma-1}]$$

for $r > 0$. This shows that vortices are also pressure/density cavities (in the polytropic case) because inertia ejects plasma out of the free spinning vortices until a pressure equilibrium is reached. More complex and realistic free vortex solutions are available [Coloni, 1991]. Dissipation usually introduces a nonzero radial velocity component in a free compressible vortex, thus mixing fluid from "outside" the vortex.

The ideal dynamics of vorticity is governed by global flow invariants (mass and momentum) as can be shown starting from the ideal fluid momentum equation. By taking its curl and using vector identities we can obtain the following form of the vorticity equation:

$$\begin{aligned} \partial_t \bar{\omega} = & -\bar{u} \cdot \bar{\nabla} \bar{\omega} + (\bar{\omega} \cdot \bar{\nabla}) \bar{u} \\ & - \bar{\omega} (\bar{\nabla} \cdot \bar{u}) + \bar{\nabla} \times \bar{f} + \frac{1}{\rho} (\bar{\nabla} \rho \times \bar{\nabla} p) \end{aligned} \quad (4)$$

Information on the time evolution of a given fluid element can be obtained using a local invariant, which can be found from (4). In a three-dimensional polytropic flow with no external force \bar{f} , the two last terms on the right hand side of equation (4) vanish. By using the convective or Lagrangian derivative D_t and the continuity equation we get the well-known vorticity transport relation

$$D_t(\bar{\omega}/\rho) = (\frac{\bar{\omega}}{\rho} \cdot \bar{\nabla}) \bar{u} \quad (5)$$

In the two-dimensional case, the vortex stretching term on the right hand side of this equation vanishes since vorticity remains perpendicular to the velocity, and by integration we get

$$\omega/\rho = \text{const} = \omega_0/\rho_0$$

This local invariant gives information on the history of the motion of individual parcels of plasma in different regions of the flow. The time evolution of vorticity following the motion of a fluid particle is strictly coupled to the evolution of density for that particle. At a given time, the regions of density lower than the original (unit) value (i.e., the darker regions along the central current sheet in Figure 5) also have lower vorticity than at initial times. Hence, the plasma that is now (at time t) inside the vortices was originally forming the original vortex sheets themselves and plasma from the sheets has migrated through mixing of vorticity throughout the central current sheet region. The plasma located where the flow was initially potential and where vorticity is now diffusing sees its density increase (white and lighter regions bordering the central current sheet in Figure 5). This remains approximately valid as long as the infinitesimal magnetic field used here is purely passive.

The departure from the local invariance of ω/ρ measures the violation of the polytropic assumption. This can be seen by setting to zero the vortex-stretching external force terms in equation (4) and applying a procedure similar to that above. We find, in the two-dimensional nonpolytropic case,

$$D_t(\bar{\omega}/\rho) = \frac{1}{\rho} (\bar{\nabla} \rho \times \bar{\nabla} p)$$

so that low-density regions such as the cavities inside the vortices are the ones that will depart most from this constant specific heat model.

We are interested in following the coherent vortex structures along the street. On the inertial-vortex-formation, or nonlinear time scales, there is little mixing of fluid from the central vortex street region with that in the outer regions, so that we must focus on macroscopic quantities which always refer to a given set of particles. Note that the fundamental

Navier-Stokes equations themselves refer to a collection of fluid particles of given identity. Hence we study plasma quantities which are represented by material (Lagrangian) integrals, not the usual (Eulerian) integrals which refer to a fixed control volume through which the plasma flows. For such applications, a useful identity can be derived from the following integral relationship [e.g., *Krall*, 1986] involving a quantity q which depends on space and time

$$\frac{d}{dt} \int_{V(t)} q d^3x = \int_{V(t)} \partial_t q d^3x + \int_{S(t)} q (\bar{u} \cdot \bar{n}) d^2x$$

(S is the surface bounding a material volume V and \bar{u} is the velocity of a surface element, \bar{n} is the outward unit vector to S). By using the divergence theorem, and taking \bar{u} to be the fluid velocity, we easily obtain the following transport theorem [e.g., *Batchelor*, 1967]:

$$\frac{d}{dt} \int_{V(t)} q d^3x = \int_{V(t)} D_t q d^3x + \int_{V(t)} (\bar{\nabla} \cdot \bar{u}) q d^3x$$

Once the material volume V is specified, this integral is a function of time alone and the two contributions to the total change in the intensive quantity q come from the change of q at some fluid point in V and the change in the orientation and shape of the material volume itself. Since enstrophy, defined by $z = (1/2)\omega^2$, is a convenient measure for the evolution of vorticity, we look at the time evolution of the total enstrophy in a volume $V(t)$ made up of a given set of fluid particles. By applying the transport relation to local enstrophy we have the time evolution of the total enstrophy Z in the volume V

$$\begin{aligned} \frac{d}{dt} Z &= \frac{d}{dt} \int_{V(t)} \frac{1}{2} \omega^2 d^3x \\ &= \int_{V(t)} \bar{\omega} \cdot D_t \bar{\omega} d^3x + \int_{V(t)} \frac{1}{2} \omega^2 (\bar{\nabla} \cdot \bar{u}) d^3x \end{aligned}$$

By using equation (4) in the first term of the right-hand side of this equation we obtain a general compressible evolution equation for the total enstrophy Z associated with a plasma volume $V(t)$

$$\begin{aligned} \frac{d}{dt} Z &= \int_{V(t)} [\bar{\omega} \cdot (\bar{\omega} \cdot \bar{\nabla}) \bar{u} - \frac{1}{2} \omega^2 (\bar{\nabla} \cdot \bar{u}) \\ &\quad + \bar{\omega} \cdot (\bar{\nabla} \times \bar{f}) + \frac{\bar{\omega}}{\rho^2} \cdot (\bar{\nabla} \rho \times \bar{\nabla} p)] d^3x \end{aligned} \quad (6)$$

The first term on the right hand side integral is the vortex stretching term that we do not consider here (since it only operates in three dimensions). In the two-dimensional polytropic approximation and neglecting body forces, this equation is reduced to the second term on the right-hand side so that compressibility is, in this ideal case, the unique source of variation for Z . More specifically, the total enstrophy of a given parcel of fluid tends to increase as it contracts and compressibility effects are more important within vortex structures. Nonpolytropic effects (which are more significant in the high vorticity and low pressure/density regions) would also contribute to changes in Z (last term in (6)). As we shall see in Section 5, the density of magnetic energy obeys a similar and useful transport equation.

5. COMPRESSIBILITY AND MAGNETIC TRANSPORT

As we have seen in Section 3, this idealized evolving compressible MHD model can yield useful information from its characteristic 'signatures' that strongly suggest the street as the process underlying the quasi-periodic meridional plasma flow [*Siregar et al.*, 1992]. We now need to test the "robustness" of the above profiles with respect to variations in the Mach number to eliminate the possibility of drawing general conclusions out of computations lying in a very restrictive region of parameter space. We tried identical runs

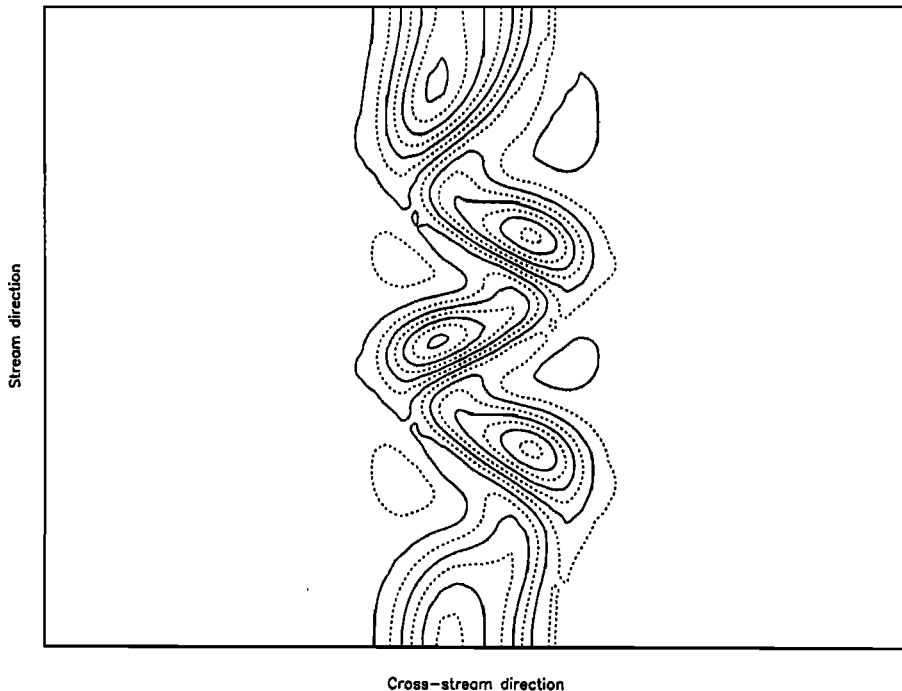


Fig. 8. Vorticity contours in the nearly incompressible $Ma = 0.2$ case at $T = 2.16$.

but with lower Mach numbers to see the effects of compressibility on this plasma flow. The local Mach number is defined by the ratio of the velocity difference $2u$ across the initial equilibrium vortex sheets to the sound speed $c = 1$ (since we start with a uniform density).

We compare the nearly incompressible regime $M_a = 0.2$ with the above results at $M_a = 0.6$ (with all other parameters being equal). At equal values of the parameter $T = t / T_0 = 2ut/\lambda$ the MHD flows reach similar states, even though different velocities are involved in each case. We first note from comparing Figures 5 and 8 at $T = 2.16$ that the coherent structures resulting from a lower Mach number reach axisymmetry in a shorter time. Most of the vorticity is distributed in individual large eddies at $M_a = 0.2$, whereas filamentary residuals of the vortex sheets still contain a large fraction of the vorticity at $M_a = 0.6$. At equivalent stages of evolution, the central current sheet preserves a much simpler structure at $M_a = 0.2$ (see Figure 9). The basic features of the meridional plasma flow profiles discussed above are preserved although, as expected, in the nearly incompressible case the density variations are much weaker and the fluctuations of the bulk plasma velocity scales according to the Mach number. The shears in the solar wind should be at considerably higher Mach numbers than used here, and this may also contribute to the anomalously low values of density fluctuations in the simulations as compared to observations.

We now turn to the evolution of the current sheet and the transport of magnetic quantities under dynamics that is essentially driven by the fluid vortex street. This allows us to address the “flux deficit” problem in the solar wind. Indeed, a deficit from the Parker field value seems to be present in the outer heliosphere when the quasi-periodic flow is observed near solar minimum (L. Burlaga, private communication, 1992). In the outer heliosphere, the Parker field has turned out of the (north-south) plane of the vortex street (considered here) so that the magnetic field component in this plane is infinitesimal and we only use it as a passive tracer.

For ecliptic solar wind applications, a current sheet is initially placed in the central region between the two vortex sheets. This allows us to locate the position of the ‘magnetic sector’ boundary. We use a small magnetic field whose energy density is negligible compared to that of the fluid ($E_{kin}/E_{mag} = 10^{-7}$) as a passive quantity in the plasma flow. The current sheet, which initially is embedded in the slow plasma region between the two vortex sheets, separates regions of opposite magnetic fields (the solar magnetic hemispheres).

In the unforced decaying evolution of the vortex street such as occurs in the solar wind, the plasma can rearrange its configuration such that its total energy is lowered, as long as a “path” exists and is “allowed” by the flow invariants, which leads from the initial state to the lower energy state. A number of constraints restrict the possible paths that the vortex street can take during its relaxation. These are the ideal local and global fluid invariants discussed above, as well as (for the passive magnetic quantities) mass and flux conservation within a magnetic flux tube; we shall discuss these effects below.

The fluid itself relaxes almost freely without having to overcome any significant magnetic forces and is dominated by the processes of vortex/antivortex repulsion and the inertial ejection of plasma from spinning vortices which creates the central expansion zone around the current sheet. We can therefore study the transport of magnetic quantities as driven

by ideal fluid relaxation but constrained by mass and flux conservation within a given tube.

Different magnetic quantities obey different evolution equations and we must look at each separately. We focus on the magnetic field itself as well as on the magnetic energy density. As is the case for vorticity, we will relate the evolution of these magnetic quantities to the changes in density. Again, during the inertial nonlinear interaction time, the mixing of quantities between the vortex street region with the outer regions is small, so that we can concentrate on given set plasma particles in the inner region. To this end, we will introduce material derivatives and integrals over volumes of a given set of plasma particles.

Starting from Maxwell’s equations and Ohm’s law one can easily derive the well-known evolution equation (equivalent to equation (3)) for the magnetic field

$$\partial_t \bar{\mathbf{b}} = \bar{\nabla} \times (\bar{\mathbf{u}} \times \bar{\mathbf{b}}) + \eta \nabla^2 \bar{\mathbf{b}} \quad (7)$$

where $\bar{\mathbf{b}}$, σ and η are the magnetic field, the conductivity and resistivity respectively. By expanding the double vector product in (7) and introducing the material derivative, we obtain the standard magnetic transport equation similar to the vorticity equation (5), namely (in the case of zero resistivity)

$$D_t (\bar{\mathbf{b}}/\rho) = \frac{1}{\rho} (\bar{\mathbf{b}} \cdot \bar{\nabla}) \bar{\mathbf{u}} \quad (8)$$

so that, as in the case of vorticity, $\bar{\mathbf{b}}/\rho$ lines are always composed of the same fluid particles, but they can rotate and stretch or be compressed. For the two-dimensional case, the main difference with vorticity is that the magnetic field is not kinematically determined from the velocity field and is not generally perpendicular to it. Hence the magnetic solutions are more complex than their vorticity counterparts. Note that the field line stretching term (right hand side of (8)) does not, in general, vanish in the magnetic case so that $\bar{\mathbf{b}}/\rho$ is not a conserved quantity as we follow a given piece of plasma, even in the two-dimensional case. In three-dimensional flows, the line stretching term can, under certain conditions, lead to dynamo action, i.e., the generation of large-scale magnetic field out of small magnetic fluctuations. However, starting from a preexisting mean field in the flow, this term can act to create or destroy the magnetic field even in two dimensions as long as there are velocity gradients along directions having a non-zero component of the field lines.

To compare the vortex street model with the solar wind, we need to work with a variable that is closer to $|\bar{\mathbf{b}}|$, a quantity measured by spacecraft. The magnetic energy density $b^2/2$ is such a quantity. To obtain its transport equation, we form the dot product of $\bar{\mathbf{b}}$ with (8) and expand the right-hand side. We get

$$D_t (b^2/2) = \bar{\mathbf{b}} \cdot (\bar{\mathbf{b}} \cdot \bar{\nabla}) \bar{\mathbf{u}} - b^2 \bar{\nabla} \cdot \bar{\mathbf{u}} \quad (9)$$

Equation (9) shows that the processes responsible for the change of magnetic energy density associated with a given piece of plasma are the stretching of field lines due to fluid motions and compressibility in the flow. In an incompressible fluid flow, line stretching becomes the only source of change for $b^2/2$ as one moves along with a parcel of plasma. Compressibility adds some freedom to the flow of plasma, but it is still constrained by magnetic flux and mass conservation within flux tubes. Indeed, in ideal MHD field lines are frozen-into the plasma, so that the evolution of a given set of plasma

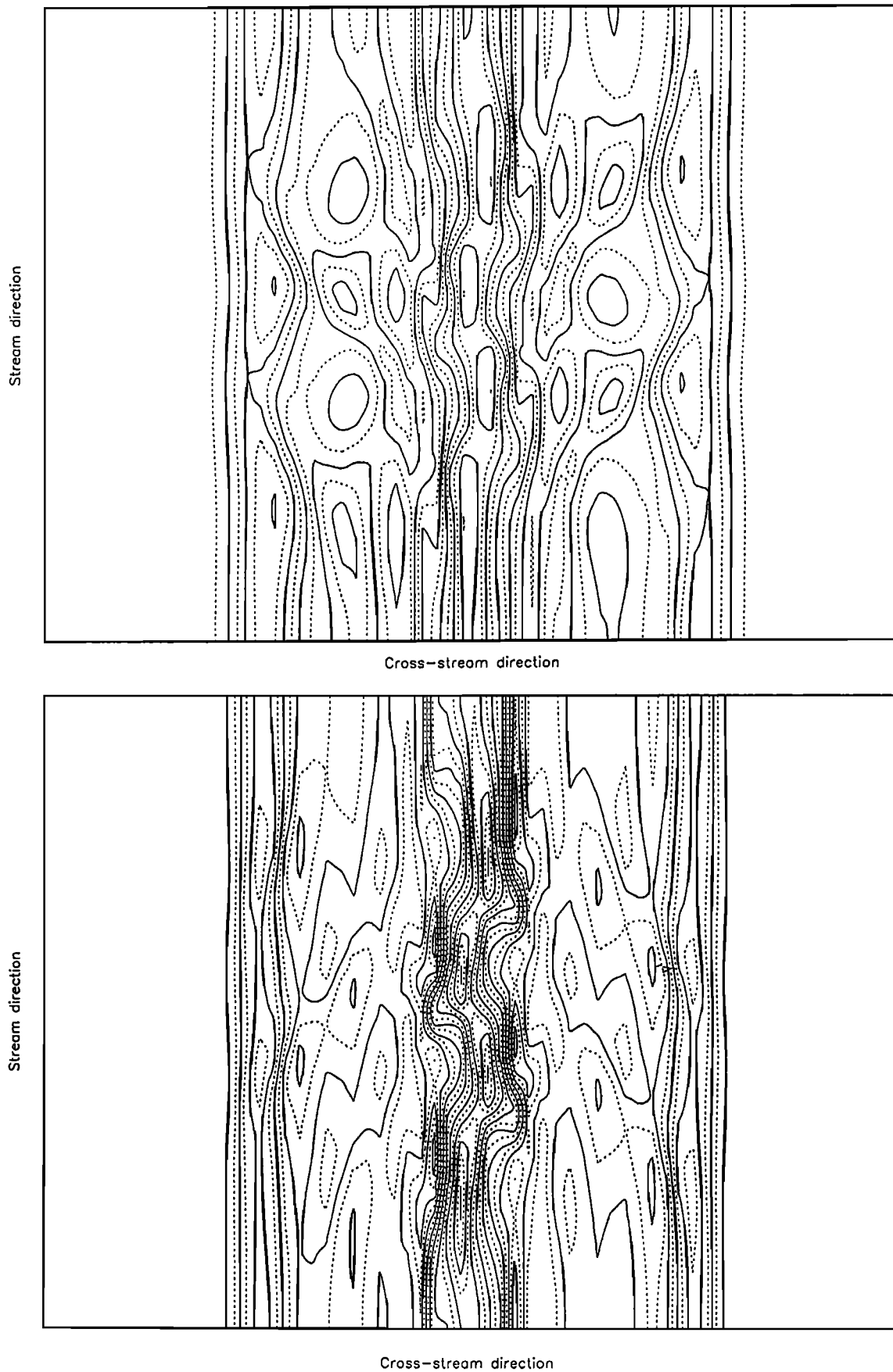


Fig. 9. The current sheet at $T=2.16$ for $Ma = 0.2$ (top) and $Ma = 0.6$ (bottom). It is not totally disrupted by the formation of the coherent structures. The current density tends to zig-zag along lines connecting the centers of the spinning plasma vortices.

particles such as those contained within a portion of a chosen flux tube, is constrained by both mass and flux conservation.

Flux and mass conservation within a flux tube correlate the two contributions in (9) but they do not determine a unique solution. Such matters, however, cannot be discussed using the differential relation (9), so that we must first establish a material integral equation for the magnetic energy density. We now determine the macroscopic time evolution for the total magnetic energy within a given parcel of plasma, such as that in a flux tube, using material integration. To obtain this relation, we use the transport theorem applied to magnetic energy density, namely

$$\frac{d}{dt} \int_{V(t)} \frac{1}{2} b^2 d^3x = \int_{V(t)} D_t \left(\frac{1}{2} b^2 \right) d^3x + \int_{V(t)} \frac{1}{2} b^2 (\bar{\nabla} \cdot \bar{u}) d^3x$$

We can finally obtain the desired magnetic energy equation using the above transport relation and equation (9) to get

$$\frac{d}{dt} E_m = \int_{V(t)} [\bar{b} \cdot (\bar{b} \cdot \bar{\nabla}) \bar{u} - \frac{b^2}{2} (\bar{\nabla} \cdot \bar{u})] d^3x \quad (10)$$

Equation (10) is similar to the evolution of enstrophy for polytropic flows (eq. (6)), but in this case, the stretching of magnetic field lines also occurs in two dimensional flows. Note that the line stretching term depends on gradients of velocity, so that it contributes to the magnetic energy through accelerations in the flow field along directions where there is a non-zero magnetic field component.

We can now discuss, using equation (10), the possible scenarios of energy transfers between fluid kinetic and magnetic energies within a parcel of plasma. First of all, how likely is a flow in which magnetic energy grows from fluid kinetic energy? The ‘alpha’ dynamo action is only possible in three dimensions and if there is a lack of mirror symmetry, or helicity, of some kind in the flow at small scales (i.e., the linkage of streamlines or vorticity tubes, magnetic flux tubes or current tubes; see *Matthaeus et al.* [1986]). It can, in this case, intensify the large scale magnetic field. The nature and amount of the various types of helicities generated in the small scales of the three dimensional vortex street flow is not clear, but here two dimensionality eliminates the possibility of a dynamo effect. It is a study which needs to be done in three dimensions and which could have consequences for the distribution of helicities in the solar wind.

We now look at the case where there is no exchange of energy between the fluid and the magnetic field within a given volume of plasma, i.e., $E_m = \text{const}$, say in a given portion of a flux tube of volume $V(t)$ in equation (10). Algebraically speaking, this leads to an exact canceling of the two terms on the right-hand side of this equation. If field lines are squeezed together, they drag the particles (which are strictly attached to each lines) along with them, increasing the density in planes perpendicular to the field lines and decreasing the density in the expansion direction parallel to the field lines, making positive, negative or zero contributions of compressibility possible. Only the total mass of plasma within the given flux tube is required to be constant in the ideal MHD case. The local density in the tube can increase, remain constant or decrease, as long as the product of the mean density times the length of the tube increases in inverse proportion to the change in its cross

section. Hence, with regard to changes in the total magnetic energy in a flux tube, the effects due to compressibility can enhance or counter the effects of field line stretching at different points in the tube. This brings us to the question of how plausible is a flow where no energy exchanges occur. It would be restricted to plasma motions that affect both the “tensile state” of the field lines and the plasma density in an exact opposite manner; this is an unlikely MHD flow, since there is no physical constraint that requires such a delicate balance.

On the other hand, a fluid vortex driven expansion is clearly active during the evolution of the street in the region along the central current sheet. Consider a cylindrical flux tube of length L , with initially constant density ρ and cross section A . Using flux conservation ($b \times A = \text{const}$), mass conservation in the tube section can expressed as $\rho L/b = \text{const}$. The expansion motion moves the plasma in the direction perpendicular to the field lines (increases A), and carries the lines with it, thus weakening the field b (by flux conservation) and decreasing ρL by the same amount as b (by mass conservation). This puts an upper bound on any possible increase in the tube length L . An upper limit on possible increase of L means an upper bound on the magnitude of the field line stretching term in equation (10). This term has more chance of being zero or negative if the fluid driven increase in A is fast enough. In the vortex street, we suggest that this expansion process can be a major contributor to the observed decrease of the magnetic energy of the plasma in the current sheet region (Figure 10). Further study is needed to investigate the direction hinted at by this admittedly simple picture.

These ideal processes are important in the earlier evolution of the vortex street, when dissipative and resistive effects are totally dominated by nonlinear inertial effects in the fluid. On this time scale the above ideal MHD discussion is relevant. The two layers of opposite vorticity tend to repel each other, broadening the street as time goes by. Since the highly vortical areas are also density cavities, the combined processes of vortex repulsion and inertial ejection of plasma result in an expansion of the plasma in the central current sheet region (density depletion is in black in Figure 5) toward the outer boundaries of the street where vorticity is close to zero (white compression regions). This expansion is quasi-perpendicular to the mean field lines and could explain the “flux deficit” in the solar wind.

For comparison with spacecraft data, Figure 10 shows the time evolution of mean magnitude of the magnetic field $\langle |b| \rangle$ in the current sheet region covering 1/8 of the total computation domain, while Figure 9b shows the corresponding evolution of mean density $\langle \rho \rangle$ in the same region. The initial drop in mean density (up to $t = 7$) occurs during the inertial vortex interaction time scale, when density cavities form inside the fast spinning vortical structures and vortex repulsion creates an expansion region.

We cannot draw quantitative conclusions on the solar wind from these computational results since many other processes occur in the solar plasma flow on these space scales, the magnetic field is used here only as a passive tracer, and the geometry is idealized and restricted by periodicity in the finite domain of computations. Nevertheless, we have shown that magnetic energy can effectively be transported to higher and lower heliocentric latitudes by the dynamics within the vortex street. We now turn to possible contributions of processes which occur on scales longer than the inertial time scales.

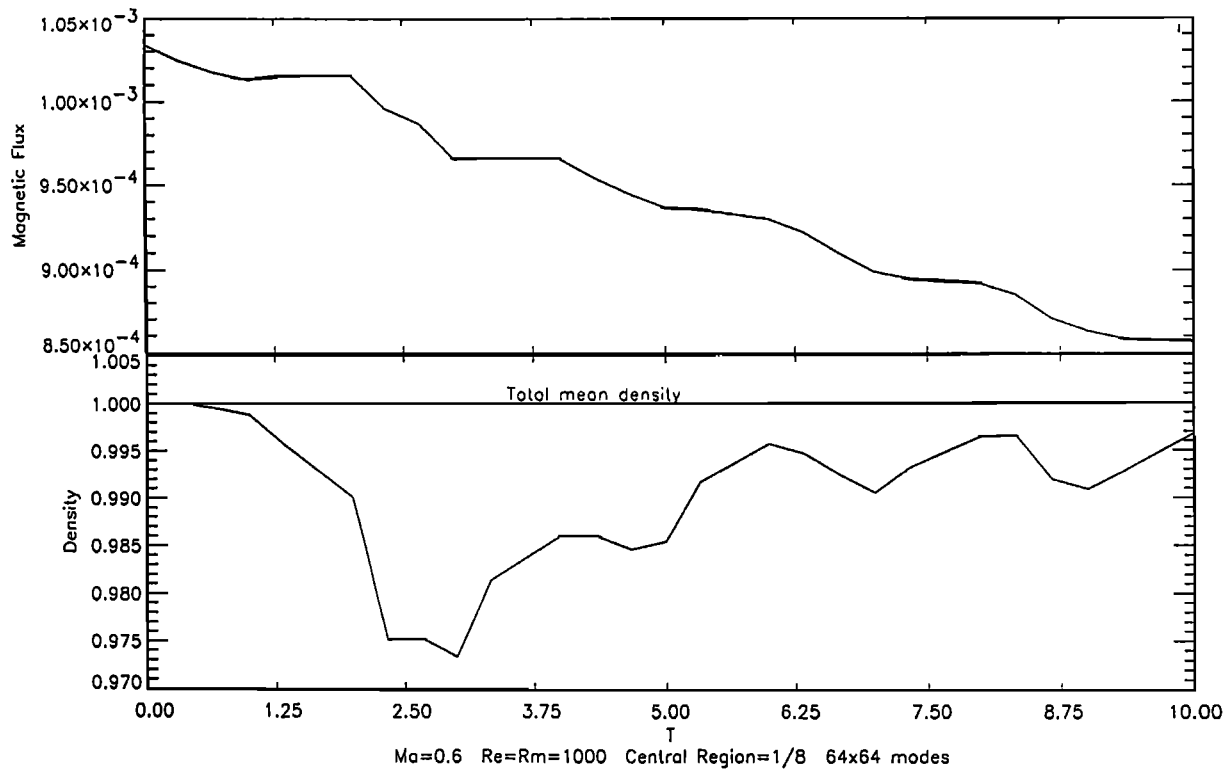


Fig. 10. Time evolution of $\langle |\bar{b}| \rangle$ and $\langle \rho \rangle$ in the central region current sheet region.

6. DISSIPATIVE AND RESISTIVE PROCESSES

In an ideally conducting plasma, the notion of field lines has a perfectly clear meaning since particles that are on a given field line at one time remain there throughout the motion. The same can be said about plasma elements within a flux tube and all the processes discussed above. The identity of field lines loses meaning as soon as the role of resistive surfaces and volumes elements become dynamically significant, partly because field lines can disappear in the presence of resistivity by reconnection and the field can diffuse with respect to the plasma. Hence, on dissipative and resistive time scales, the discussion of Section 5 becomes inapplicable.

After the nonlinear, inertial vortex formation time, the fully developed vortices decay under the influence of dissipation. As the vortex structures decay, so do their density cavities. These are long dissipative and resistive time scales on which there is also mixing of plasma driven by the coherent structures, between the inner current sheet region and the outer regions which initially contained almost no magnetic energy. These processes can explain the continued decrease of $\langle |\bar{b}| \rangle$ in the central region, even though $\langle \rho \rangle$ starts to increase in that same region. Note that these are "Eulerian" measured mean quantities, and they are therefore sensitive to the transport of quantities via mixing. To understand this mixing process, we need to look at the dynamics of a compressible dissipative vortex.

In the decay of a free compressible dissipative vortex [Colonius, 1991], there is generally a negative radial velocity component (flow into the vortex) which is related to the change of density in the vortex (the density increases to its ambient value). The origin of the radial flow into the vortex can be understood as follows: the vortex which has a lower density in its core has to gain some mass in order to decay to

the surrounding density, and this gain in mass is the origin of the radial flow into the vortex from far regions. In the vortex street, the increase of density in the vortex cores is observed during the dissipative phase and this process brings plasma from far regions which contain almost no magnetic energy into the current sheet region, thus lowering the amount of magnetic energy there.

It is also interesting that the dissipative and resistive relaxation of a fluid plasma generally gives rise to different decay rates for ideal invariants. Indeed, in more turbulent relaxation of magnetofluids the minimization of energy subject to constraints can lead to unequal decay rates for certain fluid and magnetic variables, usually ideal invariants. These "selective decay" rates [e.g., Ghosh and Matthaeus [1990]] can be understood in part by the direct and inverse turbulent cascades as the nonlinear interactions between modes can lead to two flow directions for the modal transfer of certain plasma quantities (such as the total energy and the squared vector potential). Quantities which are directly cascaded to small scales are quickly dissipated, while inversely cascaded quantities dissipate slowly since they remain far from the dissipation scales. In a later study we will address the question of whether more coherent flows such as the vortex street also display selective types of decays of ideal invariants, such as kinetic helicity in the pure fluid case.

For completeness, we briefly discuss the possible role of reconnection in the evolution of magnetic energy. In our computations, we see no large-scale changes in the magnetic field topology, but we cannot rule out the possibility of reconnection at the smallest scales in the computations. Visualizing the small scale reconnection effects is not obvious since the magnetic field energy is insignificant compared to that of the fluid. In the vortex street flow, reconnection could be significant at very small scales (compared to the vortex

structures) and in the neighborhood of the initial current sheet. Indeed, even in a fairly laminar flow such as this vortex street, magnetic fields can develop small scales. Formally, this can be seen by examining the magnetic induction equation (7). Initially, if \bar{u} and \bar{b} have comparable scales, the second term on the right-hand side is smaller than the first by a factor R_m ; but as in boundary layer theory, the dissipative term cannot be neglected in seeking the time evolution solution since it contains the highest-order derivative. The magnetic field solution can develop small scales until both terms in the right-hand side of equation (7) become comparable. In fact, small magnetic scales already exist in the central region due to the initial mean current sheet.

From a physical perspective, unsteady fluid motions eventually bring field lines of opposite polarity in contact (especially in the neighborhood of the mean current sheet) continuously creating tiny new current sheets. Hence fluid motions tend to decrease the characteristic scale of the magnetic field down to the resistive reconnection or diffusive scales. The low but still finite resistivity will quickly destroy (molecular collisional processes disrupt currents and fields) the tiny current sheets through reconnection at small scales. The generation of small-scale magnetic fields is thus suppressed at scales, say d (d is the size of the tiny current sheets), by the dissipative effects, and there is a departure from ideal MHD and frozen-in predictions. More specifically, reconnection and the violation of ideal MHD take place at scales $d = L/R_m^{1/2}$, where L are typical velocity field scales (eddy size) and R_m is the magnetic Reynolds number [see Moffatt, 1978]. So in our computations, the typical reconnection scales d are at least an order of magnitude ($R_m=10^3$) smaller than the size L of the typical energy containing eddies (the large vortices in the street; also, note that spectral algorithms have no intrinsic resistivity). In the solar wind, the ratio d/L would be even much smaller. Small scale, but continuous reconnection, could also contribute to the decrease of magnetic energy around the current sheet region.

7. CONCLUSION

The evolving vortex street model is consistent with the observations of Voyager 2 and other spacecraft [see Siregar *et al.*, 1992]. The solar rotation and coronal hole structure can create growing antisymmetric perturbations that lead to the vortex street. The essential signatures of an underlying vortex street are robust under reasonable changes the parameters that control the plasma flow. The signatures are the characteristic double-peaked maxima of the total velocity, the meridional angle, and density/pressure fluctuation maxima that spatially correlate with the rise in the total plasma velocity. There is a transport of plasma and magnetic energy away from the heliocentric equator due to vortex repulsion combined with inertial ejection of plasma within the vortices. A large enough IMF along the plasma flow direction stabilizes the shear instability and inhibits the development of the Karman street. This can explain the lack of observation of vortex street profiles before 20 AU. We conclude that a Karman street could be the mechanism underlying the observed periodic meridional flow and perhaps also the 'flux deficits' in the outer heliosphere. Plasma instabilities would maintain the growth of coherent structures along the street by extracting free energy from the two vortex layers north and south of the heliospheric equator, thus transferring a large amount of energy into the coherent modes.

Further studies should incorporate a complete exploration of parameters such as the Mach number and the possible formation of shocks. Actual inflow-outflow boundary conditions would allow the study of the evolution and spacing between the vortices along the vortex street. Three dimensionality would allow even more complex dynamical processes including azimuthal curvature effects and stretching of vortex tubes which can strengthen vorticity through angular momentum conservation. An energy equation will be needed to resolve the density/pressure degeneracy within the vortices.

Acknowledgments. All computations were performed at the NASA Center for Computational Sciences. This research was supported, in part, by the Space Physics Theory Program at the Goddard Space Flight Center. We thank L. F. Burlaga for many useful conversations.

The Editor thanks S. J. Jacobs and G. P. Zank for their assistance in evaluating this paper.

REFERENCES

- Batchelor, G. K., *An Introduction to Fluid Dynamics*, Cambridge University Press, New York, 1967.
- Burlaga, L. F., A heliospheric vortex street?, *J. Geophys. Res.*, **95**, 4333-4336, 1990.
- Colonius, T., S. K. Lele, and P. Moin, The free compressible viscous vortex, *J. Fluid Mech.*, **230**, 45-73, 1991.
- Gazis, P. R., J. D. Mihalov, A. Barnes, A. J. Lazarus, and E. J. Smith, Pioneer and Voyager observations of the solar wind at large heliocentric distances and latitudes, *Geophys. Res. Lett.*, **16**, 223, 1989.
- Gottlieb, D., and S. A. Orszag, *Numerical Analysis of Spectral Methods*, SIAM, Philadelphia, Pa., 1977.
- Ghosh, S., and W. H. Matthaeus, Relaxation processes in a turbulent compressible magnetofluid, *Phys. Fluids B*, **2** (7), 1990.
- Krall, N. A., and A. W. Trivelpiece, *Principles of Plasma Physics*, San Francisco Press, San Francisco, Calif., 1986.
- Lazarus, A. J., B. Yedidia, L. Villanueva, R. L. McNutt, and J. W. Belcher, Jr., Meridional plasma flow in the outer heliosphere, *Geophys. Res. Lett.*, **15**, 1519-1522, 1988.
- Matthaeus, W. H., M. L. Goldstein, and S. R. Lantz, The alpha dynamo parameter and measurability of helicities in magnetohydrodynamic turbulence, *Phys. Fluids*, **29** (5), 1504, 1986.
- McNutt, R., Meridional plasma flow in the outer heliosphere, *Geophys. Res. Lett.*, **15**, 1523-1526, 1988.
- Moffatt, H. K., Magnetic field generation in electrically conducting fluids, *Cambridge University Press*, New York, 1978.
- Pizzo, V. J., and B. E. Goldstein, Meridional transport of magnetic flux in the solar wind between 1 and 10 AU: A theoretical analysis, *J. Geophys. Res.*, **92**, 7241, 1987.
- Roberts, D. A. and Goldstein, M. L., Turbulence and waves, Contributions in solar-planetary relationships, U.S. National Report 1987-1990, 1991.
- Siregar E., Roberts D.A., and Goldstein M.L., Magnetohydrodynamics of interacting vortex sheets, in the *Proceedings from the Chapman Conference on micro and meso-scale phenomena in space plasmas, Kauai, Hawaii*, in press, 1992.
- Siregar E., D.A., Roberts, and M. L. Goldstein, The formation of vortex streets through the nonlinear interactions of vortex sheets in a two-dimensional compressible flow, *Geophys. Res. Lett.*, **19**, 1427, 1992.
- Ting A. C., W. H. Matthaeus, and D. Montgomery, Turbulent relaxation processes in magnetohydrodynamics, *Phys. Fluids*, **29** (10), 3261, 1986.
- Tritton D.J., *Physical Fluid Dynamics*, Van Nostrand Reinhold, New York, 1977.

M. L. Goldstein, D. Aaron Roberts, and E. Siregar, Laboratory for Extraterrestrial Physics, NASA Goddard Space Flight Center, Greenbelt, MD 20771.

(Received October 30, 1992;
revised March 9, 1993;
accepted April 13, 1993.)